Distribution of stress state in the Nankai subduction zone, southwest Japan and a comparison with Japan Trench

Weiren Lin[1,2*], Timothy B. Byrne[3], Masataka Kinoshita[4,5], Lisa C. McNeill[6], Chandong Chang[7], Jonathan C. Lewis[8], Yuzuru Yamamoto[9], Demian M. Saffer[10], J. Casey Moore[11], Hung-Yu Wu[5], Takeshi Tsuji[12], Yasuhiro Yamada[5], Marianne Conin[13], Saneatsu Saito[5], Takatoshi Ito[14], Harold J. Tobin[15], Gaku Kimura[16], Kyuichi Kanagawa[17], Juichiro Ashi[18], Michael B. Underwood[19], Toshiya Kanamatsu[20]

[1] Graduate School of Engineering, Kyoto University, Kyoto, Japan

[2] Kochi Institute for Core Sample research, Japan Agency for Marine-Earth Science and Technology, Nankoku, Japan

[3] Center for Integrative Geosciences, University of Connecticut, Storrs, Connecticut, USA.

[4] Earthquake Research Institute, The University of Tokyo, Tokyo, Japan

[5] Institute for Research on Earth Evolution, Japan Agency for Marine-Earth Science and Technology, Yokohama, Japan.

[6] Southampton Oceanography Centre, University of Southampton, Southampton, UK.

[7] Department of Geology, Chungnam National University, Daejeon, Korea

[8] Department of Geoscience, Indiana University of Pennsylvania, Indiana, Pennsylvania, USA.

[9] Department of Mathematical Science and Advanced Technology, Japan Agency for Marine and Earth Science and Technology, Yokohama, Japan

[10] Department of Geosciences and Center for Geofluids, Geomechanics, and Geohazards, The Pennsylvania State University, Pennsylvania, USA

[11] Earth and Planetary Sciences Department, University of California, Santa Cruz, California, USA

[12] International Institute for Carbon-Neutral Energy Research, Kyushu University, Fukuoka, Japan

[13] University of Lorraine – ENSMN, Nancy, France

[14] Institute of Fluid Science, Tohoku University, Sendai, Japan

[15] Department of Geoscience, Univ. Wisconsin — Madison, Madison, USA

[16] Department of Earth and Planetary Science, The University of Tokyo, Tokyo, Japan

[17] Department of Earth Sciences, Chiba University, Chiba, Japan.

[18] Atmosphere and Ocean Research Institute, The University of Tokyo, Tokyo, Japan

[19] Department of Geological Science, University of Missouri, Columbia, USA

[20] Research and Development Center for Earthquake and Tsunami, Japan Agency for Marine‐Earth Science and Technology, Yokosuka, Japan

*Corresponding author:
Address: Graduate School of Engineering, Kyoto University, C1-1-109
C-cluster, Kyoto Daigaku Katsura, Nishikyo-ku, Kyoto 615-8540, Japan.
E-mail: lin@kumst.kyoto-u.ac.jp Fax: +81 75 383 3203

Key Words: Stress state, Nankai subduction zone, Japan Trench, Ocean drilling

Abstract: To better understand the distribution of three dimensional stress states in the Nankai subduction zone, southwest Japan, we review various stress-related investigations carried out in the first and second stage expeditions of the Nankai Trough Seismogenic Zone Experiment (NanTroSEIZE) by the Integrated Ocean Drilling Program (IODP) and compile the stress data. Overall, the maximum principal stress σ_1 in the shallower levels (<~1km) is vertical from near the center of forearc basin to near the trench and; the maximum horizontal stress S_{Hmax} (interpreted to be the intermediate principal stress σ_2) is generally parallel to the plate convergence vector. The exception to this generalization occurs along the shelf edge of the Nankai margin where S_{Hmax} is along strike rather than parallel to the plate convergence vector. Reorientation of the principal stresses at deeper levels (e.g., >~1km below seafloor or in underlying accretionary prism) with σ_1 becoming horizontal is also suggested at all deeper drilling sites. We also

55 make a comparison of the stress state in the hanging wall of the frontal plate-interface
56 between Site C0006 in the Nankai and Site C0019 in the Japan Trench subduction zone
57 drilled after the 2011 Mw9.0 Tohoku-Oki earthquake. In the Japan Trench, the
58 comparison between stress state before and after the 2011 mega-earthquake shows that
59 the stress changed from compression before the earthquake to extension after the
60 earthquake. As a result of the comparison between the Nankai Trough and Japan Trench,
61 a similar current stress state with trench parallel extension was recognized at both
62 C0006 and C0019 sites. Hypothetically, this may indicate that in Nankai Trough it is still
63 in an early stage of the interseismic cycle of a great earthquake which occurs on the
64 décollement and propagates to the toe (around site C0006).
65
66 **1. Introduction**
67 Stress and earthquakes are known to be interrelated: stress triggers earthquakes and
68 earthquakes alter the shear and normal stresses on surrounding faults (Stein, 1999;
69 Seeber and Armbruster, 2000; Hardebeck, 2004; Ma et al., 2005; Lin et al., 2007). On the
70 other hand, the stresses both on the fault and in the formation gradually build up in the
71 interseismic period (Kanamori and Brodsky, 2001). The Nankai Trough Seismogenic
72 Zone Experiment (NanTroSEIZE), a comprehensive scientific drilling project conducted

73 by the Integrated Ocean Drilling Program (IODP) in the Nankai subduction zone,
74 southwest Japan, is designed to investigate the mechanics of the subduction megathrust
75 through drilling and a wide range of allied studies (Tobin and Kinoshita, 2006; Tobin et
76 al., 2009a). In this area, Mw 8.0 class great earthquakes repeat at intervals of 100–200
77 years as a result of the convergence of the Philippine Sea and Eurasian plates (Ando,
78 1975; Fig. 1). The last two great earthquakes in the Nankai subduction zone occurred in
79 1944 (Tonankai, M 8.0-8.3) and 1946 (Nankai, M 8.1-8.4), generating tsunamis and
80 causing significant damage in southwest Japan (Kanamori 1972). The NanTroSEIZE
81 project sampled and continues to monitor the characteristics of the seismogenic zone
82 during the interseismic interval. In contrast, IODP expedition 343 to the Japan Trench
83 (also referred to as the Japan Trench Fast Drilling Project or JFAST), was conducted just
84 after a great earthquake, about 13 months after the 2011 Mw 9.0 Tohoku-Oki, Japan
85 earthquake (Mori et al., 2012; Chester et al., 2012; Fig. 1).

86 Establishing the in situ stress state along active subduction zones is critical for
87 understanding the accumulation and release of most of Earth's seismic energy
88 (Lallemand and Funiciello, 2009). Determination of in situ stress is one of the most
89 important scientific objectives of both NanTroSEIZE and JFAST, and also one of the
90 major goals of the IODP as the seismogenic parts of plate margins are often only

accessible through drilling. First, we review various stress-related investigations carried out in association with NanTroSEIZE stages 1 and 2. We then compare the present-day stress states in the frontal part of the plate-interface at the Nankai and Japan Trench subduction zones and propose hypotheses on the temporal and spatial evolution of stresses in the frontal plate-interface in Nankai, SW Japan.

2. Stress estimates and direct measurements from stage 1 and 2 of the NanTroSEIZE drilling project

The multi-stage scientific drilling project NanTroSEIZE, conducted by the drilling vessel D/V *Chikyu,* began in 2007 with IODP expedition 314 and is continuing with planned deep riser drilling in the coming years (Kinoshita et al., 2008; Hirose et al., 2013). To date more than 10 drilling sites have been drilled along the NanTroSEIZE transect with at least one vertical borehole(s) at each site. This transect is approximately orthogonal to the Nankai Trough axis (plate boundary) (Fig. 2, 3 and 4a and Table 1).

In the first stage of NanTroSEIZE (2007–2008), borehole wall images obtained by logging while drilling (LWD) technology yielded regional patterns of stress orientations and magnitudes through observations of drilling-induced compressive failures (borehole breakouts) and tensile fractures (DITFs) (e.g., Tobin et al., 2009b; Chang et al,

109 2010; Lin et al., 2010a; Moore et al., 2011; Lee et al., 2013). This stage involved five
110 drilling sites in three structural settings in which LWD was performed: the frontal thrust
111 at the toe of the accretionary prism, Site C0006; the megasplay hanging wall and
112 footwall, Sites C0010, C0004 and C0001, and the seaward edge of the Kumano forearc
113 basin, Site C0002 (Fig. 2, 3 and 4a). These regional studies were followed by more
114 detailed core-based analyses and geophysical studies, including interpretation of
115 high-resolution seismic reflection data and S-wave splitting that provided a
116 three-dimensional understanding of the stress field and the evolution of stresses
117 through time (Byrne et al., 2009; Kimura et al., 2011; Tsuji et al., 2011a; Lewis et al.,
118 2013; Moore et al., 2013; Sacks et al., 2013; Conin et al., 2014). Taken together, these
119 results show that at all sites except C0004 and C0010, the maximum principal stress σ_1
120 is vertical at shallow levels and that the orientation of the intermediate principal
121 stress σ_2 changes from trench perpendicular at C0006 and C0001 to trench parallel at
122 C0002. At sites C0004 and C0010 σ_1 is interpreted possibly to be horizontal and
123 approximately parallel to the plate convergent direction.
124 In the second stage of NanTroSEIZE (2009-2010), D/V *Chikyu* carried out the first
125 riser drilling in IODP history at Site C0009 of Expedition 319. This expedition targeted
126 the hanging wall above the high slip region of the 1944 Tonankai earthquake (Saffer *et*

127 *al.*, 2009). The borehole penetrated the Kumano forearc basin sediments and the
128 underlying accretionary prism; and was the deepest drilling (~1.6 km) during the first
129 and second stages of NanTroSEIZE. In a depth range from approximately 700 mbsf
130 (meters below seafloor) to the target depth of 1600 mbsf, wireline logging included a
131 borehole caliper and a fullbore formation microimager (FMI) that provided resistivity
132 images. From the borehole images and caliper data, borehole breakouts and DITFs were
133 identified and the horizontal stress orientations were obtained (Saffer et al., 2009; Lin et
134 al., 2010a; Wu et al., 2012). Due to limited azimuthal coverage (~50%) of the wellbore
135 walls by FMI, the width of breakouts was not well constrained, and therefore no reliable
136 information about stress magnitudes could be extracted from the wellbore failures.
137 The first hydraulic fracturing experiments in the scientific ocean drilling history
138 also were carried out using two techniques at Site C0009. The first, an "extended leak-off
139 test", was conducted as part of drilling operations and provided a measurement of
140 minimum principal stress magnitude at ~708 mbsf (Saffer et al., 2013; Lin et al., 2008).
141 The second technique, a "two dual-packer hydraulic fracture test" was conducted using
142 Modular Dynamic Tester (MDT) tool (Ito et al., 2013; Saffer et al., 2013; Haimson and
143 Cornet, 2003), and yielded two additional measurements of in situ minimum principal
144 stress magnitude: one at ~877 mbsf and a less reliable determination at ~1534 mbsf.

145 Drill core samples were also recovered in a ~80m depth interval in mudstones
146 interpreted as either the uppermost accretionary prism or a paleo-slope basin. Anelastic
147 strain recovery (ASR) measurements on core samples were used to determine the
148 three-dimensional stress orientations by the same method as Byrne et al. (2009) (Lin et
149 al., 2010b). In addition, results of a "walkaround" vertical seismic profiling (VSP)
150 experiment recorded at Site C0009 and conducted by D/V *Chikyu* and R/V *Kairei* showed
151 a clear anisotropy in P wave velocity and amplitude, and documented S wave splitting.
152 These data have also been interpreted as indicators of horizontal stress orientations
153 (Tsuji et al., 2011b).

154 During IODP expeditions 322 in stage 2, two reference sites were drilled on the
155 incoming Philippine Sea Plate: Site C0012, located ~31 km seaward of the trench on
156 basement high to sample a condensed sedimentary section, and Site C0011, ~22 km
157 seaward of the trench designed to sample the section at a basement low. LWD resistivity
158 images documented borehole breakouts and provide an indication of horizontal
159 principal stress orientations at Site C0011 (Expedition 322 Scientists, 2010; Wu et al.,
160 2013). Site C0012 was not drilled with LWD; however, ASR measurements on core
161 samples yielded constraints on stress states in both the oceanic crust (basalt) and the
162 sedimentary cover (Yamamoto et al., 2013).

3. Results of Stage 1 drilling, Nankai subduction zone, SW Japan

3.1. C0001

Borehole breakouts, tensile fractures and core-scale faults are present in the upper half of the boreholes at Site C0001 and provide constraints on the orientation, ratios and magnitudes of the principal stresses (Expedition 314 Scientists, 2009a). The maximum horizontal stress S_{Hmax} orientation determined from borehole breakouts and tensile fractures consistently trend ~335° throughout the hole, although Chang et al. (2010) proposed that the stress regime changes with depth, likely due to increasing S_{Hmax} (Fig. 2). At shallow levels (<~500 mbsf) S_{Hmax} is interpreted to be σ_2 and smaller in magnitude than the vertical stress, reflecting a normal faulting regime. Consolidation and triaxial compression tests of slope sediments in the uppermost ~200 mbsf also suggest horizontal effective stresses are ~41% of the vertical effective stress consistent with a normal faulting regime (Song et al., 2011). Stress inversion of core-scale faults from C0001 provide a measure of the three-dimensional stress state at relatively shallow levels and also show normal faulting with extension parallel to the margin (Lewis et al., 2013). These results are consistent with faulting patterns observed in seismic reflection data as well as with the borehole breakout data that show σ_2

subparallel to the plate convergence vector. Lewis et al. (2013) also recognized an older suite of faults that, when inverted for stress orientations, show σ_1 trending northwest, parallel to the plate convergence vector. Chang et al. (2010) interpret S_{Hmax} at deeper levels (>~500 mbsf) to be σ_1, reflecting a change with depth from normal faulting to strike-slip, or possibly thrusting. Unfortunately, sediment cores were not retrieved from deeper levels where the principal stresses appear to permutate.

3.2. C0002

Site C0002, which penetrated the Kumano forearc basin and the upper part of the underlying accretionary prism, also shows a consistent orientation of borehole breakouts with depth and a possible permutation of stresses with depth. S_{Hmax} determined from breakouts, however, trend northeast, approximately perpendicular to S_{Hmax} at C0001, which is only 10 km to the southeast (Fig. 2 and 3). Analysis of the breakouts, results from ASR experiments and inversion of core-scale faults show a normal faulting regime in the forearc sequence with the minimum principal stress σ_3 nearly parallel to the plate convergence vector and perpendicular to the shelf break. These results are consistent with numerous margin parallel normal faults observed in seismic reflection data (Gulick et al., 2010; Moore et al., 2013; Sacks et al., 2013). Many of the faults also cut the seafloor, suggesting that they are active or recently active, and

199 the lack of growth data suggests that the transition to an extension dominated basin
200 occurred less than ~1 Ma ago (Gulick et al, 2010). Sacks et al. (2013) and Moore et al.
201 (2013) also show that there is a systematic change from any an early phase of generally
202 trench-parallel extension that started before 0.44 Ma to trench-normal extension
203 associated with faults that often cut the seafloor. These results are consistent with
204 observations of core-scale fault populations that show a change from NE-SW extension
205 to NW-SE extension (Expedition 315 Scientists, 2009). Chang et al. (2010) propose that
206 the stress regime changes below the forearc sediments with S_{Hmax} becoming σ_1,
207 suggesting a change from normal faulting to strike-slip or thrusting similar to the change
208 proposed for Site C0001. The stress states at the two sites, however, are still
209 fundamentally different as the borehole breakouts, and therefore S_{Hmax}, are
210 perpendicular even at the deepest structural levels. In fact, the trend of S_{Hmax}, which is
211 interpreted to be σ_1 in the deeper levels of C0002, suggests margin-parallel shortening
212 rather than margin perpendicular shortening as interpreted for the deeper levels of
213 C0001 (Fig. 2).

214 *3.3. C0004*

215 Site C0004 penetrated the megasplay fault, which appears to have slipped coseismically
216 during the 1944 earthquake (Sakaguchi et al., 20011b) and borehole breakouts show

consistent trends throughout the hole with S_{Hmax} trending northwest-southeast, approximately parallel to S_{Hmax} at C0001 (Expedition 314 Scientists, 2009b; Fig. 2). Site C0004 is only a few kms from C0001 and Byrne et al. (2009) assumed a relatively homogeneous stress field and proposed that S_{Hmax} at this site represented σ_2 rather than σ_1. More recent analyses of borehole breakouts, however, by Olcott and Saffer (2012) and Yamada and Shibanuma (2015) suggest that S_{Hmax} at this site possibly represents σ_1 consistent with a reverse or strike-slip faulting regime. They described that the magnitude of the vertical stress S_v may be smaller than that of S_{Hmax} but within the possible range of S_{hmin} (see Fig. 4 in Yamada and Shibanuma, 2015).

3.4. C0006

Site C0006 penetrated and sampled the hanging wall of the frontal thrust and borehole breakouts, anelastic strain and core-scale faults provide a more complete picture of the stress state than at C0004. Borehole breakouts occur throughout most of the hole although they appear much more weakly developed than at the other three sites. The breakouts trend 060° consistent with results from Sites C0001 and C004, indicating that S_{Hmax} trends about 330°, approximately parallel to the plate convergence vector (Expedition 314 Scientists, 2009c). ASR on a core sample from the hanging wall and inversion of the youngest suite of core-scale faults show a steeply plunging σ_1 with σ_3

235 trending northeast, indicating normal faulting and margin-parallel extension, similar to
236 Site C0001 at shallow depths (Fig. 6b). Interpretations of the stress field around Site
237 C0006 using a slip deficit model also indicate a normal faulting regime (Fig. 6a; Wu et al.,
238 2013), and conjointly a significant erosion at the top of the slope sediments can be
239 observed (Strasser et al, 2011; Conin et al, 2011). Anisotropy of magnetic susceptibility
240 data (Byrne et al., 2009; Kitamura et al., 2010) and suites of core-scale structures that
241 pre-date the normal faults show an earlier phase of margin-perpendicular shortening,
242 which is also similar to the observations from Site C0001 (Lewis et al. 2013).

243 *3.5. C0007*

244 Site C0007, located less than a kilometer seaward of Site C0006 and a few hundred
245 meters from the deformation front, was drilled after coring at Site C0006 failed to reach
246 the frontal thrust (Fig. 3). Although the holes drilled at Site C0007 were not logged, so
247 borehole images are not available, observations of cores indicate a deformation history
248 similar to the history documented at Site C0006; that is, early northwest-southeast
249 shortening followed by normal faulting. In addition, vitrinite reflectance measurements
250 of samples from the frontal thrust show anomalously high temperatures, suggesting that
251 the fault moved co-seismically (Sakaguchi et al., 2011a). Sites C0006 and C0007 together
252 therefore may represent an analogous setting to Site C0019 in the Tohoku area which

253 also sampled the front thrust after it slipped co-seismically.

254

255 **4. Results from Stage 2, Nankai subduction zone, SW Japan**

256 *4.1. C0009*

257 At Site C0009, direct measurements of σ_3 via hydraulic fracturing tests and leak-off test
258 (LOT) indicate that the stress regime changes from a normal faulting stress regime in the
259 Kumano basin sediments to a possible strike-slip or thrusting stress regime in the
260 underlying slope basin or accretionary wedge, to a depth of at least ~1600 mbsf similar
261 to the change at Site C0001 (Fig. 2; Lin et al., 2010b; Ito et al., 2013; Saffer et al., 2013;
262 Wu et al., 2013). Estimates of stress magnitude from the width of borehole breakouts at
263 Site C0002 suggested a similar pattern, i.e. changing from a normal faulting stress
264 regime in the basin sediments to a strike slip or thrust faulting regime in the underlying
265 accretionary prism to the depth of ~1380 mbsf (the lower limit of breakout occurrence
266 in borehole C0002A) (Tobin et al., 2009a; Byrne et al., 2009; Chang et al., 2010; Lee et al.,
267 2013).

268 *4.2. C0010*

269 Site C0010 is located a few km along strike from Site C0004 and, similar to C0004,
270 penetrated the hanging wall and footwall of the megasplay, one of primary drilling

targets of the NanTroSEIZE. Shipboard analysis of the borehole breakouts showed a consistent pattern above the megasplay with the maximum horizontal stress trending NW-SE. McNeill et al. (2010) noted that the megasplay corresponds to a seismic reflector with negative polar, suggesting a reduction in velocity and/or density in the footwall. They also recognized an abrupt change in orientation of the breakouts across the megasplay and proposed that the fault zone represented a sharp mechanical discontinuity. Although Olcott and Saffer (2012) proposed that σ_1 remained horizontal beneath in the footwall similar to the results from C0004, they also documented a shift to lower stress magnitudes in the footwall, based on the widths of borehole breakouts.

4.3. C0011 and C0012

At Site C0011, the orientation of S_{Hmax} was determined by borehole breakouts observed in a narrow depth interval (~600 – 650 mbsf, Expedition 322 Scientists, 2010) and is oblique to the plate convergence vector. Although estimates of stress magnitude are strongly dependent on assumed rock strength parameters, a normal faulting stress regime was suggested on the basis of wellbore breakout widths at ~610 mbsf (Wu et al., 2013).

At Site C0012, which is the most seaward input site and occurs on the crest of a prominent basement high (Kashinosaki Knoll), ASR results suggest a normal faulting

289 regime in the sedimentary sequence, with S_{Hmax} oriented WNW-ESE (Yamamoto et al.,
290 2013). In contrast, ASR analysis of a core sample of oceanic basement basalt shows a
291 strike slip or a reverse faulting stress regime, with the maximum horizontal stress
292 orientated northeast – southwest approximately parallel to the trough axis. The
293 basement stress orientation could be the result of hinge extension during bending of the
294 Philippine Sea plate, either in association with subduction or with the formation of an
295 anticline during intraoceanic thrusting (Yamamoto et al., 2013).
296

297 **5. Discussion: Nankai Margin**

298 Although the drilling depths in stages 1 and 2 are relatively shallow (<~1.6 km at Site
299 C0009), the results suggest important trends in both depth and map view. For example,
300 observations at many of the sites suggest a change from a normal faulting regime at
301 shallow structural levels to strike-slip or thrusting at deeper levels. These results
302 suggest that gradients in topography may play an important role in defining the state of
303 stress. Deeper drilling, like the programs completed as part of Expedition 348 which
304 penetrated to ~3 kmbsf at Site C0002 and the future NanTroSEIZE expeditions planned
305 to drill to > 5 kmbsf in the same borehole will better define change in stress states with

306 depth and provide a clearer understanding of how stress changes temporally and
307 spatially in the prism.

308 The above review suggests two general patterns for the states of stress at
309 relatively shallow levels: First, σ_1 appears to be vertical at all sites except in the hanging
310 wall of the megasplay at Sites C0004 and C0010 where σ_1 is interpreted to be
311 sub-horizontal and parallel to the plate convergence vector. Second, the maximum
312 horizontal stresses S_{Hmax} appear to be parallel to the plate convergence vector except
313 near the seaward edge of the Kumano Basin at Site C0002 where σ_3 is parallel to the
314 plate convergence vector.

315 A possible explanation for the reorientation of σ_1 at C0004 and C0010 may be
316 that the sediments being carried in the hanging wall are relatively strong and capable of
317 supporting plate tectonic stresses. The occurrence of an extensional regime at higher
318 structural levels where slope sediments are dominant (e.g., Site C0001) and the
319 identification of a relatively weak footwall (Olcott and Saffer, 2012; McNeill et al, 2010)
320 are consistent with this interpretation. We therefore propose that the hanging wall of the
321 megasplay is relatively strong and supports a compressional stress state that is
322 consistent with plate convergence. In contrast, the transmission of the stresses
323 associated with plate convergence appears to be less effective in the slope sequence

where σ_2 is observed to be parallel to the plate convergence vector and in the footwall where stress magnitudes decrease and possibly reorient. Drilling and sampling of core-scale faults across the décollement at Site 808 during the Ocean Drilling Program (ODP) Leg 131 along the Muroto transect also documented a reorientation of stresses (Lallemant et al., 1993). At this site σ_1 is sub-horizontal and NW-trending above the décollement, similar to the results from C0004 and C0010, and but sub-vertical below the décollement (Lallemant et al., 1993). One possibility is that the stresses below the megasplay have also been reoriented and σ_1 is vertical (Fig. 3) or they record a transition in stress states.

At C0002 the reorientation of σ_3 relative to the regional pattern may reflect gravitation collapse of the prism as the décollement weakens either continuously or during large earthquakes as suggested for the Tohoku region (McKenzie and Jackson, 2012; Kimura et al., 2012; Tsuji et al., 2013). A seismic reflection profile running NW–SE and including Site C0002 displays a clear sequence of trough-parallel normal faults in the basin sediments consistent with the maximum horizontal stress orientation data (e.g. Tobin et al., 2009a). Sacks et al. (2013) (and see also Moore et al., 2013) analyzed this regional-scale fault system in more detail and recognized two patterns of extension – an early phase of generally northeast-southwest, or margin-parallel, extension and a later

342 phase of trench-perpendicular extension that is concentrated on the seaward edge of the
343 basin. The fact that trench-perpendicular extension appears to be limited to the area of
344 the shelf edge, which is both relatively far from the plate interface and at the topographic
345 crest, is consistent with the hypothesis that gradients in topography (including effects of
346 the "notch" proposed by Martin et al., 2010) are important in defining the state of stress
347 along the margin. Theoretical studies as well as analog and numerical models also
348 suggest that variations in the strength of the décollement below the wedge can lead to
349 extension in the overlying accretionary wedge. For example, Haq and Davis (2008) show
350 that for wedges with a ductile base, accretion can lead to over steepened topography and
351 flow at lower structural levels, which drive trench-perpendicular extension (i.e., normal
352 faulting) at higher structural levels. In fact, several authors have proposed that a regional
353 low-velocity zone beneath the Nankai margin represents weak, and probably
354 overpressured sediments (Park et al., 2010; Byrne et al. 2009; Bangs et al., 2009; Kamei
355 et al., 2012; Kitajima & Saffer, 2012) that may act like the ductile lower crust in the
356 analog models.

357 The above hypothesis for the pattern of regional-scale stresses, however, fails to
358 consider the possible change in stresses associated with the earthquake cycle. For
359 example, this region of the Nankai margin experienced a major earthquake and tsunami

360 in 1944; and Sakaguchi et al. (2011a), based on maturation studies of vitrinite collected
361 from fault zones sampled at Sites C0004 and C0007, proposed that megasplay and
362 décollement slipped during the earthquake(s). Presumably, for some period before, and
363 up to the beginning of the earthquake the state of stress in the hanging wall would have
364 been compressional with σ_1 orientated sub-parallel to the plate convergence vector. The
365 evidence from all of the sites along the Kumano transect where the principal stress
366 orientations can be determined, however, shows a normal faulting regime, at least at
367 shallow structural levels and excluding Sites C0004 and C0010 which sampled the
368 hanging wall of the megasplay. These data also show that the rocks failed exclusively by
369 normal faulting; that is, there is no evidence in the cores or seismic reflection data for
370 alternating periods of extension and compression that could be interpreted as stress
371 permutations associated with an earthquake cycle. For example, observation from Site
372 C0002 and detailed studies of the deformation history in the Kumano Basin (Lewis et al.,
373 2013 and Sacks et al., 2013, respectively) show an early phase of trench-parallel
374 extension followed by a phase of trench-perpendicular extension. Neither data set shows
375 stress permutations where the principal stresses switch multiple times, for example over
376 several earthquake cycles. At least two explanations are possible, either: 1) all of the late
377 stage normal faults formed after the last earthquake (e.g., after 1944) due to stress

relaxation and stress permutations or 2) the stress states vary during the seismic cycle (e.g., σ_1 alternates between horizontal and vertical from one cycle to the next) (Wang and Hu, 2006; Conin et al., 2012; Kinoshita and Tobin, 2013; Sacks et al., 2013; Hashimoto et al., 2014), but during an earthquake, failure is accommodated only or primarily by slip on major thrust faults and not on core-scale faults. After a major earthquake, the associated stress drop and relaxation leads to decrease in S_{Hmax}, such that the vertical stress S_v becomes σ_1, depending on the local stress field. Hsu et al. (2009) recently proposed an interpretation similar to the second alternative (#2 above) for stress permutations before and after the 1999 Chichi earthquake in Taiwan.

6. Stress states at the Japan Trench

6.1. IODP drilling Site C0019 and ODP Sites 1150 and 1151

The Japan Trench lies along the eastern edge of Japan and marks the boundary where the Pacific plate subducts beneath the Okhotsk plate (or North American plate) at ~8 cm/year (Loveless and Meade, 2010) (Fig. 1). The Tohoku-Oki earthquake (Mw 9.0) occurred on March 11, 2011 and was followed by a huge tsunami (Simons et al., 2011; Ide et al., 2011) that flooded many coastal regions of northeast Japan, taking over 18,000 lives. Planning for IODP Expedition 343 (informally called the "Japan Trench Fast Drilling

396 Project" or JFAST) began soon after the earthquake with the primary goal of better
397 understanding the stress and slip history along the fault. To this end, the goals of the
398 expedition were to: 1) test the possibility that coseismic slip on a major fault generated
399 frictional heat; 2) to investigate stress state on the fault and 3) retrieve samples from the
400 proposed fault zone. To achieve these goals IODP expedition 343 conducted a rapid
401 response drilling program about 13 months after the earthquake. The expedition
402 successfully penetrated and sampled the frontal fault at a depth of ~820 mbsf at IODP
403 Site C0019 where coseismic displacements were relatively large (~50 m) (Mori et al.,
404 2012; Chester et al., 2012). Site C0019 is located ~93 km seaward from the epicenter of
405 the mainshock of the Tohoku-Oki earthquake and ~6 km landward of the trench axis (Fig.
406 4b and 5).

407 In addition to the JFAST site, Sites 1150 and 1151, also located near the source
408 area of the Tohoku-Oki earthquake, were drilled during ODP Leg 186 in 1999 prior to the
409 earthquake (Lin et al., 2011) (Fig. 4b). Lin et al. (2011) integrated FMS images with
410 caliper data to interpret the orientation of S_{Hmax} at the two sites.

411 *6.2. Results from C0019*

412 Lin et al. (2013) analyzed LWD data collected by JFAST at Site C0019 (Fig. 4b)
413 and integrated these data with compressive strength and core-based observations to

414 determine the stress state and to infer stress history at this site. Although borehole
415 breakouts are present throughout the hanging wall of the plate boundary, they are show
416 a wide range in orientations at shallow structural levels (<500 mbsf), suggesting that
417 S_{Hmax} and S_{hmin} are close in magnitude, and/or that S_{Hmax} orientation is highly variable
418 with depth. At deeper levels (>500 mbsf) S_{Hmax} shows a clear trend to the northwest
419 (319 ± 23°), which is sub parallel to the plate convergence vector of 292° at this location
420 (Fig.4b; Argus et al., 2011). Lin et al. (2013) also used the width of the borehole
421 breakouts and the results of initial shipboard experiments on the unconfined
422 compressive strength (UCS) of sediments from two depth intervals to determine the
423 stress magnitudes. Their results show that the frontal part of the prism above the plate
424 boundary fault is in, or close to, a normal faulting regime (Fig. 6c). These results contrast
425 with core-scale observations, however, that show dominantly thrusting and horizontal
426 shortening with only limited evidence of extension at relatively shallow structural levels.
427 Based on these results, the authors suggested a distinct coseismic stress change from a
428 reverse faulting stress regime before the earthquake to a normal faulting stress regime
429 after the earthquake (Fig. 7). This interpretation is well-consistent with Hasegawa et al.
430 (2012).

431 *6.3. Results from ODP Sites 1150 and 1151*

FMS and caliper data from Sites 1150 and 1151 were used to define the orientation of S_{Hmax} at these two sites, which were drilled prior to the Tohoku-Oki earthquake. The FMS images showed the development of drilling induced tensile fractures (DITF) and borehole breakouts at deeper structural levels (e.g., > 700mbsf) and the caliper data provide a general constraint on the orientation of borehole breakouts. Although there is variability between the two sites, the combined data set shows S_{Hmax} trending northwest, generally parallel to the plate convergence vector (Lin et al., 2011) (Fig. 4b). Based on the presence of DITFs at both sites and significant seismic activity associated with northwest-southeast directed shortening, Lin et al. (2011) concluded that the hanging of the plate boundary in this area possibly was in a thrusting regime before the 2011 earthquake.

7. Comparison between Nankai and Japan Trench

The general comparison of the Nankai and Tohoku margins presented above shows that the margins share important similarities as well as at least one critical difference (Fig. 5). First, available data suggest that both margins are dominated by an extensional stress regime with a vertically oriented maximum principal stress. Extension along the Tohoku area is show by the dominance of normal faulting aftershocks in the hanging wall above

450 the décollement (Tsuji et al., 2013) as well as the in situ stress data from Site C0019.
451 Extension along Nankai is documented by seismic reflection data along the shelf edge
452 and observations from 3 drill sites that span the accretionary prism. Horizontal
453 compression may occur at deeper levels and in the hanging wall of the megasplay, but
454 normal faulting appears to be the dominant pattern. The second similarity is that both
455 margins can be divided into inner and outer wedges separated by a regionally significant
456 normal fault or a complex system of normal and oblique slip faults. At Tohoku, a
457 landward dipping normal fault with significant offset separates a deep-sea terrace from
458 the upper, middle and low slope that define the accretionary wedge. At Nankai, the
459 seaward edge of the forearc basin is marked by relatively intricate set of normal faults
460 associated with a graben-like structure that marks shelf edge. Some of the normal faults
461 may also have oblique slip that accommodate strike-parallel motion related to
462 moderately oblique plate convergence (Martin et al., 2010). Finally, one critical
463 difference appears to be the presence of a megasplay in the accretionary prism of the
464 Nankai margin and the apparent absence of similar structures along the Tohoku margin.
465 Interestingly, the similarities of the two margins are also the primary
466 characteristics of margins that typically produce tsunami earthquakes (Tsuji et al., 2013;
467 McKenzie and Jackson, 2012). For example, recent theoretical studies (McKenzie and

468 Jackson, 2012) as well as recent observations from Tohoku (Tsuji et al., 2013) suggest
469 tsunami genic earthquakes result from the simultaneous slip along the décollement and
470 a landward-dipping normal fault or a suite of normal faults that separate the inner and
471 outer wedges. McKenzie and Jackson (2012) also propose that displacements on these
472 regional-scale faults and the seaward motion of the outer wedge is driven by the release
473 of gravitational potential energy as well as elastic strain. Although McKenzie and Jackson
474 (2012) do not address what processes cause the décollement and the normal fault to fail
475 simultaneously, Kimura et al. (2012) suggest that progressive dewatering of underthrust
476 sediments along the Tohoku margin lead to failure and "runaway" slip along the
477 décollement probably weakened by over pore pressure (e.g. Tobin and Saffer, 2009;
478 Kitajima et al., 2012; Hashimoto et al., 2013; Tsuji et al., 2014). Tsuji et al. (2013), based
479 on sea floor observations of extension cracks and heat flow anomalies, also propose that
480 normal faulting in the hanging wall occurred simultaneously with slip on the
481 décollement. Along the Nankai margin, the décollement is also interpreted to be
482 anomalously weak and the seaward edge of the Kumano Basin is deformed exclusively
483 by normal faults, suggesting a tectonic setting similar to Tohoku. One possibility,
484 therefore, is that during a historic great earthquake, which also produced a tsunami

485 along southwest Japan, slip occurred simultaneously on normal faults in the hanging
486 wall and along the décollement.

487 A complication to this interpretation is that models of the 1944 tsunami suggest
488 that a significant amount of the coseismic slip occurred on the megasplay rather than the
489 décollement (Tanioka and Satake, 2001; Cummins et al., 2002). However, Sakaguchi et al.
490 (2011a), based on observations from Site C0007 which is near the toe of the prism, show
491 that the décollement also moved co-seismically, although the timing of co-seismic slip is
492 unknown. If the model proposed for Tohoku (McKenzie and Jackson, 2012) also applies
493 to the 1944 event along the Kumano transect, then movement along both the megasplay
494 and the décollement must have driven forward motion of the accretionary wedge.

495 We therefore propose that the two margins represent similar states between
496 tsunami earthquakes, although there are differences. Following this interpretation, the
497 stress state of the accretionary wedge, including the frontal plate interface builds up
498 from a normal faulting stress regime just after a large earthquake to a reverse faulting
499 regime before the next earthquake. In other words, the tectonic horizontal stress caused
500 by plate convergence gradually builds up during the interseismic period and dynamically
501 drops during an earthquake consistent with the conventional stress accumulation
502 fundamental model (e.g. see Kanamori and Brodsky, 2001). Following this interpretation,

503 both Sites C0006 (Nankai) and Site C0019 (Tohoku) appear to be in the early stages of
504 the interseismic cycle with σ_1 is vertical and that S_{Hmax} (interpreted to be σ_2) is generally
505 parallel to the plate convergence vector (Fig. 6). In Nankai margin, more than 60 years
506 have passed from the previous M8-class earthquake propagated through the megasplay
507 fault to the time of drilling at C0006 (2007), but the time length from the previous great
508 earthquake occurred on the décollement and propagated to C0006 is unknown.
509 Hypothetically, the stress state may indicate that in Nankai margin, it is still in an early
510 stage of the interseismic cycle of a great earthquake which occurs on the décollement
511 and propagates to the toe, even cuts the seafloor.
512
513
514 **Acknowledgments.** This research used data provided by the IODP. The authors
515 gratefully acknowledge helpful discussions with NanTroSEIZE scientists and JFAST
516 scientists and the support provided by EPMs, logging staffs, and laboratory technicians
517 of the expeditions. We really thank the two reviewers, Serge Lallemand and Yoshitaka
518 Hashimoto, for their careful reading and constructive comments which helped us to
519 improve this manuscript. Part of these works were supported by Grants-in-Aid for
520 Scientific Research 25287134 (JSPS), and 21107006 (MEXT), Japan.
521
522

References

Ando, M., 1975. Source mechanisms and tectonic significance of historical earthquakes along the Nankai Trough, Japan. Tectonophysics 27, 119—140.

Apel, E. V., Burgmann, R., Steblov, G., Vasilenko, N., King, R., & Prytkov, A., 2006. Independent active microplate tectonics of northeast Asia from GPS velocities and block modeling, Geophys. Res. Lett. 33, L11303, http://dx.doi.org/10.1029/2006GL026077.

Argus, D. F., Gordon, R. G., & DeMets, C., 2011. Geologically current motion of 56 plates relative to the no-net-rotation reference frame, Geochem. Geophys. Geosyst. 12, Q11001, http://dx.doi.org/10.1029/2011GC003751.

Bangs, N., Moore, G.F., Gulick, S. P. S., Pangborn, E.M., Tobin, H.J., Kuramoto, S., & Taira, A., 2009. Broad, weak regions of the Nankai Megathrust and implications for shallow coseismic slip. Earth and Planetary Science Letters 284, 44-49.

Byrne, T., & Fisher, D., 1990, Evidence for a weak and overpressured décollement beneath sediment-dominated accretionary prisms. Journal of Geophysical Research 95, 9081-9097.

Byrne, T., Lin W., Tsutsumi, A., Yamamoto, Y., Lewis, J., Kanagawa, K., Kitamura, Y., Yamaguchi, A. & Kimura, G., 2009. Anelastic strain recovery reveals extension across SW Japan subduction zone, Geophys. Res. Lett. 36, L01305, http://dx.doi.org/ 10.1029/2009GL040749.

Chang, C., McNeill, L.C., Moore, J.C., Lin, W., Conin, M. & Yamada, Y., 2010. In situ stress state in the Nankai accretionary wedge estimated from borehole wall failures, Geochem. Geophys. Geosyst. 11, Q0AD04 (2010), http://dx.doi.org/10.1029/2010GC003261.

Chester, F.M., Mori, J.J., Toczko, S., Eguchi, N. & the Expedition 343/343T Scientists., 2012. Japan Trench Fast Drilling Project (JFAST). IODP Prel. Rept. 343/343T, http://dx.doi.org/10.2204/iodp.pr.343343T.2012.

Conin, M., Henry, P., Bourlange, S., Raimbourg, H., & Reuschle, T., 2011. Interpretation of porosity and LWD resistivity from the Nankai accretionary wedge in the light of clay physicochemical properties: evidence for erosion and local overpressuring, Geochem. Geophys. Geosyst. 12, Q0AD07.

Conin, M., Henry, P., Godard, V. & Bourlange, S., 2012. Splay fault slip in a subduction margin, a new model of evolution. Earth and Planetary Science Letters 341, 170-175 (2012).

Conin, M., Bourlange, S., Henry, P., Boiselet, A. & Gaillot, P., 2014. Distribution of resistive and conductive structures in Nankai accretionary wedge reveals contrasting stress

559 paths, Tectonophysics 611, 181-191.
560 Cummins, P.R., Hori, T. and Kaneda, Y., 2001. Splay fault and megathrust earthquake slip
561 in the Nankai Trough, Earth Planets Space 53, 235–241.
562 Expedition 314 Scientists, 2009a. Expedition 314 Site C0001. *In* Kinoshita, M., Tobin, H.,
563 Ashi, J., Kimura, G., Lallement, S., Screaton, E.J., Curewitz, D., Masago, H., Moe, K.T.,
564 and the Expedition 314/315/316 Scientists, Proc. IODP 314/315/316: Washington,
565 DC (Integrated Ocean Drilling Program Management International, Inc.).
566 http://dx.doi.org/10.2204/iodp.proc.314315316.113.2009
567 Expedition 314 Scientists, 2009b. Expedition 314 Site C0004. *In* Kinoshita, M., Tobin, H.,
568 Ashi, J., Kimura, G., Lallement, S., Screaton, E.J., Curewitz, D., Masago, H., Moe, K.T.,
569 and the Expedition 314/315/316 Scientists, Proc. IODP 314/315/316: Washington,
570 DC (Integrated Ocean Drilling Program Management International, Inc.).
571 http://dx.doi.org/10.2204/iodp.proc.314315316.116.2009
572 Expedition 314 Scientists, 2009c. Expedition 314 Site C0006. *In* Kinoshita, M., Tobin, H.,
573 Ashi, J., Kimura, G., Lallemant, S., Screaton, E.J., Curewitz, D., Masago, H., Moe, K.T.,
574 and the Expedition 314/315/316 Scientists, Proc. IODP 314/315/316: Washington,
575 DC (Integrated Ocean Drilling Program Management International, Inc.).
576 http://dx.doi.org/10.2204/iodp.proc.314315316.118.2009
577 Expedition 315 Scientists, 2009. Expedition 315 Site C0002. *In* Kinoshita, M., Tobin, H.,
578 Ashi, J., Kimura, G., Lallemant, S., Screaton, E.J., Curewitz, D., Masago, H., Moe, K.T.,
579 and the Expedition 314/315/316 Scientists, Proc. IODP 314/315/316: Washington,
580 DC (Integrated Ocean Drilling Program Management International, Inc.).
581 http://dx.doi.org/10.2204/iodp.proc.314315316.124.2009
582 Expedition 319 Scientists, 2010. Site C0010. *In* Saffer, D., McNeill, L., Byrne, T., Araki, E.,
583 Toczko, S., Eguchi, N., Takahashi, K., and the Expedition 319 Scientists, Proc. IODP
584 319: Tokyo (Integrated Ocean Drilling Program Management International, Inc.).
585 http://dx.doi.org/10.2204/iodp.proc.319.104.2010
586 Expedition 322 Scientists, 2010. Site C0011. *In* Saito, S., Underwood, M.B., Kubo, Y., and
587 the Expedition 322 Scientists, Proc. IODP 322: Tokyo (Integrated Ocean Drilling
588 Program Management International, Inc.).
589 http://dx.doi.org/10.2204/iodp.proc.322.103.2010
590 Gulick, S. P., Bangs, N., Moore, G., Ashi, J., Martin, K. M., Sawyer, D., Tobin, H., Kuramoto,
591 S., & Taira, A., 2010. Rapid forearc basin uplift and megasplay fault development
592 from 3D seismic images of Nankai margin off Kii Peninsula, Japan: Earth and
593 Planetary Science Letters 300, 55-62,
594 http://dx.doi.org/10.1016/j.epsl.2010.09.034.

595 Haimson, B.C. & Cornet, F.H., 2003. ISRM suggested methods for rock stress
596 estimation—Part 3: Hydraulic fracturing (HF) and/or hydraulic testing of
597 pre-existing fractures (HTPF). Int. J. Rock Mech. Min. Sci. 40, 1011–1020.
598 Hardebeck, J. L., 2004. Stress triggering and earthquake probability estimates, J. Geophys.
599 Res. 109. B04310, http://dx.doi.org/10.1029/2003JB002437.
600 Haq, S. S. B. & Davis, D. M., 2008. Extension during active collision in thin-skinned
601 wedges: Insights from laboratory experiments: Geology 36, 475-478.
602 Hasegawa, A., Yoshida, K., Asano, Y., Okada, T., Iinuma, T., and Ito, Y., 2012. Change in
603 stress field after the 2011 great Tohoku–Oki earthquake. Earth Planet. Sci. Lett.,
604 355-356, 231-243, http://dx.doi.org/10.1016/j.epsl.2012.08.042.
605 Hashimoto, Y., Doi, N., and Tsuji, T., 2013. Difference in acoustic properties at
606 seismogenic fault along a subduction interface: Application to estimation of
607 effective pressure and fluid pressure ratio, Tectonophysics, 600, 134-141,
608 http://dx.doi.org/10.1016/j.tecto.2013.03.016
609 Hashimoto, Y., Eida, M., & Ueda. Y., 2014. Changes in paleostress state along a subduction
610 zone preserved in an on-land accretionary complex, the Yokonami mélange in the
611 Cretaceous Shimanto Belt, Kochi, southwest Japan, Tectonics, 33, 2045–2058,
612 http://dx.doi.org/10.1002/2013TC003487.
613 Heki K., & Miyazaki, S., 2001. Plate convergence and long-term crustal deformation in
614 Central Japan, Geophys. Res. Lett. 28**,** 2313–2316.
615 Hirose, T., Saffer, D.M., Tobin, H.J., Toczko, S., Maeda, L., Kubo, Y., Kimura, G., Moore, G.F.,
616 Underwood, M.B., and Kanagawa, K., 2013. NanTroSEIZE Stage 3: NanTroSEIZE
617 plate boundary deep riser 3. IODP Sci. Prosp. 348.
618 http://dx.doi.org/10.2204/iodp.sp.348.2013
619 Hsu, Y.-J., Yu, S.-B., Simons, M., Kuo, L.-C. & Chen, H.-Y., 2009. Interseismic crustal
620 deformation in the Taiwan plate boundary zone revealed by GPS observations,
621 seismicity, and earthquake focal mechanisms. Tectonophysics
622 http://dx.doi.org/10.1016/j.tecto.2008.11.016.
623 Ide, S., Baltay, A. & Beroza, G.C., 2011. Shallow dynamic overshoot and energetic deep
624 rupture in the 2011 *M*w 9.0 Tohoku-Oki earthquake. Science 332 1426-1429,
625 http://dx.doi.org/10.1126/science.1207020.
626 Ienaga, M., McNeill, L.C., Mikada, H., Saito, S., Goldberg, D. & Moore, J.C., 2006. Borehole
627 image analysis of the Nankai Accretionary Wedge, ODP Leg 196: Structural and
628 stress studies, Tectonophysics 426, 207–220,
629 http://dx.doi.org/10.1016/j.tecto.2006.02.018
630 Ito, T., Funato, A., Lin, W., Doan, M.-L., Boutt, D. F., Kano, Y., Ito, H., Saffer, D., McNeill, L.C.,

631 Byrne, T. & Moe, K.T., 2013. Determination of stress state in deep subsea formation
632 by combination of hydraulic fracturing in situ test and core analysis: A case study in
633 the IODP Expedition 319. J. Geophys. Res. Solid Earth 118,
634 http://dx.doi.org/10.1002/jgrb.50086.
635 Kamei, R., Pratt, R.G., & Tsuji, T., 2012. Waveform tomography imaging of a megasplay
636 fault system in the seismogenic Nankai subduction zone, Earth and Planetary
637 Science Letters 317-318, 343-353.
638 Kanamori, H., 1972. Tectonic implications of the 1944 Tonankai and the 1946 Nankaido
639 earthquakes, Phys. Earth Planet. Inter. 5, 129–139.
640 Kanamori, H. & Brodsky, E., 2001. The physics of earthquakes, Physics Today 54(6), 34,
641 http://dx.doi.org/10.1063/1.1387590.
642 Kimura, G., Moore, G., Strasser, M., Screaton, E., Curewitz, D., Streiff, C., & Tobin, H., 2011,
643 Spatial and temporal evolution of the megasplay fault in the Nankai Trough:
644 Geochem. Geophys. Geosyst. 12, Q0A008,
645 http://dx.doi.org/10.1029/2010GC003335.
646 Kimura G. et al., 2012. Runaway slip to the trench due to rupture of highly pressurized
647 megathrust beneath the middle trench slope: The tsunamigenesis of the 2011
648 Tohoku earthquake off the east coast of northern Japan, Earth Planet. Sci. Lett.
649 339-340, 32-45, http://dx.doi.org/10.1016/j.epsl.2012.08.042.
650 Kinoshita, M., Tobin, H., Moe, K.T. & the Expedition 314 Scientists, 2008. NanTroSEIZE
651 Stage 1A: NanTroSEIZE LWD Transect. IODP Prel. Rept. 314.
652 http://dx.doi.org/10.2204/iodp.pr.314.2008.
653 Kinoshita, M. and Tobin, H., 2013. Interseismic stress accumulation at the locked zone of
654 Nankai Trough seismogenic fault off Kii Peninsula, Tectonophysics 600, 153-164.
655 http://dx.doi.org/10.1016/j.tecto.2013.03.015.
656 Kitajima, H., and Saffer, D.M., 2012. Elevated pore pressure and anomalously low stress
657 in regions of low frequency earthquakes along the Nankai Trough subduction
658 megathrust, Geophys. Res. Lett. 39, L23301,
659 http://dx.doi.org/10.1029/2012GL053793.
660 Kitamura, Y., Kanamatsu, T. and Zhao, X., 2010. Structural evolution in accretionary
661 prism toe revealed by magnetic fabric analysis from IODP NanTroSEIZE Expedition
662 316, Earth and Planetary Science Letters 292, 221-230.
663 Kodaira S. *et al*., 2012. Coseismic fault rupture at the trench axis during the 2011
664 Tohoku-oki earthquake, Nature Geoscience 5, 646-650,
665 http://dx.doi.org/10.1038/NGEO1547.
666 Lallemand, S., and Funiciello F., 2009. Subduction Zone Geodynamics, Springer, Berlin.

667 Lallemant, S.J., Byrne, T., Maltman, A., Karig, D., and Henry, P., 1993. Stress tensors at the
668 toe of the Nankai accretionary prism: An application of inverse methods to
669 slickenlined faults, Proceedings of the Ocean Drilling Program, Scientific Results 131,
670 103-122.
671 Lee, H., Chang, C., Ong, S.H., & Song I., 2013. Effect of anisotropic borehole wall failures
672 when estimating in situ stresses: A case study in the Nankai accretionary wedge,
673 Marine and Petroleum Geology 48, 411-422,
674 http://dx.doi.org/10.1016/j.marpetgeo.2013.09.004
675 Lewis, J., Byrne, T., and Kanagawa, K., 2013, Evidence for mechanical decoupling of the
676 upper plate at the Nankai subduction zone: Constraints from core-scale faults at
677 NantroSEIZE Sites C0001 and C0002: Geochem. Geophys. Geosyst. 14, 620–633,
678 http://dx.doi.org/10.1029/2012GC004406.
679 Lin, W. et al., 2007. Current Stress State and Principal Stress Rotations in the Vicinity of
680 the Chelungpu Fault Induced by the 1999 Chi-Chi, Taiwan, earthquake, Geophys. Res.
681 Lett. 34, L16307, http://dx.doi.org/10.1029/2007GL030515.
682 Lin, W., Yamamoto, K., Ito, H., Masago, H. & Kawamura, Y., 2008. Estimation of Minimum
683 Principal Horizontal Stress from an Extended Leak-off Test onboard the *Chikyu*
684 drilling vessel and Suggestions for Future Test Procedures, Scientific Drilling No.6,
685 43-47, http://dx.doi.org/10.2204/iodp.sd.6.06.2008.
686 Lin, W. et al., 2010a. Present-day principal horizontal stress orientations in the Kumano
687 forearc basin of the southwest Japan subduction zone determined from IODP
688 NanTroSEIZE drilling Site C0009, Geophys. Res. Lett. 37, L13303,
689 http://dx.doi.org/10.1029/2010GL043158.
690 Lin, W., Byrne, T., Yamamoto, Yuhji & Yamamoto, Yuzuru. 2010b. Preliminary results of
691 three-dimensional stress orientation in the accretionary prism in Nankai
692 Subduction Zone, Japan by anelastic strain recovery measurements of core samples
693 retrieved from IODP NanTroSEIZE Site C0009, Abstract T13A-2151 presented at
694 2010 Fall Meeting, AGU, San Francisco, Calif., 13-17 Dec.
695 Lin, W., Saito, S., Sanada, Y., Yamamoto, Y., Hashimoto, Y. & Kanamatsu, T., 2011. Principal
696 horizontal stress orientations prior to the 2011 M_w 9.0 Tohoku-Oki, Japan,
697 earthquake in its source area. Geophys. Res. Lett. 38, L00G10,
698 http://dx.doi.org/10.1029/2011GL049097.
699 Lin, W., Conin, M., Moore, J.C., Chester, F.M., Nakamura, Y., Mori, J.J., Anderson, L., Brodsky,
700 E.E., Eguchi, H. & Expedition 343 Scientists, 2013. Stress state in the largest
701 displacement area of the 2011 Tohoku-Oki earthquake, Science 339, 687-690,
702 http://dx.doi.org/ 10.1126/science.1229379.

703 Loveless, J.P. & Meade B.J., 2010. Geodetic imaging of plate motions, slip rates, and
704 partitioning of deformation in Japan, J. Geophys. Res. 115, B02410,
705 http://dx.doi.org/10.1029/2008JB006248.
706 Ma, K.-F., Chan, C.-H. & Stein, R.S., 2005. Response of seismicity to Coulomb stress
707 triggers and shadows of the 1999 Mw=7.6 Chi-Chi, Taiwan, earthquake, J. Geophys.
708 Res. 110, B05S19, http://dx.doi.org/10.1029/2004JB003389.
709 McKenzie, D. and Jackson, J., 2012. Tsunami earthquake generation by the release of
710 gravitational potential energy, Earth Planet. Sci. Lett. 345–348, 1–8.
711 Martin, K.M., Gulick, S.P.S., Bangs, N.L.B., Moore, G.F., Ashi, J., Park, J-O., Kuramoto, S. &
712 Taira, A., 2010. Possible strain partitioning structure between the Kumano fore-arc
713 basin and the slope of the Nankai Trough accretionary prism, Geochem. Geophys.
714 Geosyst. 11, Q0AD02, http://dx.doi.org/10.1029/2009GC002668.
715 McNeill L.C. et al., 2004. Deformation and in situ stress in the Nankai Accretionary Prism
716 from resistivity-at-bit images, ODP Leg 196, Geophys. Res. Lett. 31, L02602,
717 http://dx.doi.org/10.1029/2003GL018799.
718 McNeill L.C., Saffer, D.M., Byrne, T., Araki, E., Toczko, S., Eguchi, N., Takahashi, K. &
719 Expediion 319 Scientists, 2010, IODP Expedition 319, NanTroSEIZE Stage 2: First
720 IODP Riser Drilling Operations and Observatory Installation Towards
721 Understanding Subduction Zone Seismogenesis, Scientific Drilling 10, 4-13,
722 http://dx.doi.org/10.2204/iodp.sd.10.01.2010.
723 Miyazaki, S. & Heki, K., 2001. Crustal velocity field of southwest Japan: subduction and
724 arc-arc collision. J. Geophys. Res. 106(B3), 4305–4326,
725 http://dx.doi.org/10.1029/2000JB900312
726 Moore, G.F., Park, J.-O., Bangs, N.L., Gulick, S.P., Tobin, H.J., Nakamura, Y., Sato, S., Tsuji, T.,
727 Yoro, T., Tanaka, H., Uraki, S., Kido, Y., Sanada, Y., Kuramoto, S., and Taira, A., 2009.
728 Structural and seismic stratigraphic framework of the NanTroSEIZE Stage 1
729 transect. *In* Kinoshita, M., Tobin, H., Ashi, J., Kimura, G., Lallement, S., Screaton, E.J.,
730 Curewitz, D., Masago, H., Moe, K.T., and the Expedition 314/315/316 Scientists,
731 Proc. IODP 314/315/316: Washington, DC (Integrated Ocean Drilling Program
732 Management International, Inc.).
733 http://dx.doi.org/10.2204/iodp.proc.314315316.102.2009
734 Moore, G. F., Boston, B. B., Sacks, A. F., and Saffer, D. M., 2013, Analysis of Normal Fault
735 Populations in the Kumano Forearc Basin,Nankai Trough, Japan: 1 Multiple
736 Orientations and Generations of Faults from 3-D Coherency Mapping: Geochemistry,
737 Geophysics, Geosystems 114, 1989–2002, http://dx.doi.org/10.1002/ggge.20119.
738 Moore, J.C., Chang, C., Mcneill, L.C., Moe, T.K., Yamada, Y. & Huftile, G., 2011. Growth of

739 borehole breakouts with time after drilling: implications for state of stress,
740 NanTroSEIZE transect, SW Japan. Geochemistry, Geophysics, Geosystems 12,
741 Q04D09. http://dx.doi.org/10.1029/2010GC003417.
742 Mori, J.J., Chester, F.M., Eguchi, N. & Toczko, S., 2012. Japan Trench Fast Earthquake
743 Drilling Project (JFAST). IODP Sci. Prosp. 343,
744 http://dx.doi.org/10.2204/iodp.sp.343.2012.
745 Olcott, K., and Saffer, D., 2012. Constraints on in situ stress across the shallow megasplay
746 fault offshore the Kii Peninsula, SW Japan from borehole breakouts, Abstract
747 T13A-2576 presented at 2012 Fall Meeting, AGU, San Francisco, Calif., 3-7 Dec.
748 Ozawa, S., Nishimura, T., Suito, H., Kobayashi, T., Tobita, M., & Imakiire, T., 2011.
749 Coseismic and postseismic slip of the 2011 magnitude-9 Tohoku-Oki earthquake,
750 Nature 475, 373–376, http://dx.doi.org/10.1038/nature10227.
751 Park, J.-O. Fujie, G., Wijerathne, L., Hori, T., Kodaira, S., Fukao, Y., Moore, G.F., Bangs, N.L.,
752 Kuramoto, S., & Taira, A., 2010. A low-velocity zone with weak reflectivity along the
753 Nankai subduction zone. Geology 38, 283-286,
754 http://dx.doi.org/10.1130/G30205.1.
755 Sacks, A., Saffer, D. M., & Fisher, D., 2013, Analysis of normal fault populations in the
756 Kumano forearc basin, Nankai Trough, Japan: 2. Principal axes of stress and strain
757 from inversion of fault orientations: Geochemistry, Geophysics, Geosystems 14,
758 1973-1988.
759 Saffer, D.M. et al., 2009. NanTroSEIZE Stage 2: NanTroSEIZE riser/riserless observatory.
760 IODP Prel. Rept. 319. http://dx.doi.org/10.2204/iodp.pr.319.2009.
761 Saffer, D.M., Flemings, P.B., Boutt, D., Doan, M.-L., Ito, T., McNeill, L., Byrne, T., Conin, M.,
762 Lin, W., Kano, Y., Araki, E., Eguchi, N. & Toczko S., 2013. In situ stress and pore
763 pressure in the Kumano Forearc Basin, offshore SW Honshu from downhole
764 measurements during riser drilling, Geochem. Geophys. Geosyst. 14, 1454-1470,
765 http://dx.doi.org/10.1002/ggge.20051.
766 Saito, S., Underwood, M.B., & Kubo, Y., 2009. NanTroSEIZE Stage 2: subduction inputs.
767 IODP Sci. Prosp. 322. http://dx.doi.org/10.2204/iodp.sp.322.2009.
768 Sakaguchi, A., Chester, F., Curewitz, D., Fabbri, O., Goldsby, D., Kimura, G., Li, C.-F., Masaki,
769 Y., Screaton, E.J., Tsutsumi, A., Ujiie, K. & Yamaguchi A., 2011a. Seismic slip
770 propagation to the updip end of plate boundary subduction interface faults:
771 Vitrinite reflectance geothermometry on Integrated Ocean Drilling Program
772 NanTroSEIZE cores, Geology 39, 395–398, http://dx.doi.org/10.1130/G31642.1.
773 Sakaguchi, A., Kimura, G., Strasser, M., Screaton, E.J., Curewitz, D. & Murayama, M., 2011b.
774 Episodic seafloor mud brecciation due to great subduction zone earthquakes,

775 Geology 39, 919–922, http://dx.doi.org/10.1130/G32043.1.
776 Seeber, L. & Armbruster, J.G., 2000. Earthquakes as beacons of stress change, Nature 407,
777 69-72.
778 Simons, M., Minson, S.E., Sladen, A., Ortega, F., Jiang, J., Owen, S.E., Meng, L., Ampuero, J-P.,
779 Wei, S., Chu, R., Helmberger, D.V., Kanamori, H., Hetland, E., Moore A.W. & Webb, F.
780 H., 2011. The 2011 Magnitude 9.0 Tohoku-Oki Earthquake: Mosaicking the
781 Megathrust from Seconds to Centuries, Science 332, 1421-1425,
782 http://dx.doi.org/10.1126/science.1206731.
783 Sella, G.F., Dixon, T.H., Mao, A., 2002. REVEL: a model for recent plate velocities from
784 space geodesy. Journal of Geophysical Research 107 (B4), 2081.
785 http://dx.doi.org/10.1029/2000JB000033.
786 Song, I., Saffer, D.M., Flemings, P.B., 2011. Mechanical characterization of slope
787 sediments: constraints on in situ stress and pore pressure near the tip of the
788 megasplay fault in the Nankai accretionary complex. Geochemistry, Geophysics,
789 Geosystems 12, Q0AD17. http://dx.doi.org/10.1029/2011GC003556.
790 Stein, R.S., 1999. The role of stress transfer in earthquake occurrence, Nature 402,
791 605-609.
792 Strasser, M., Moore, G. F. Kimura, G. Kopf, A. J. Underwood, M. B. Guo, J. and Screaton E. J.,
793 2011. Slumping and mass transport deposition in the Nankai fore arc: Evidence
794 from IODP drilling and 3-D reflection seismic data, Geochem. Geophys. Geosyst. 12,
795 Q0AD13, http://dx.doi.org/10.1029/2010GC003431.
796 Tanioka, Y. and Satake, K., 2001. Coseismic slip distribution of the 1946 Nankai
797 earthquake and aseismic slips caused by the earthquake, Earth Planets Space 53,
798 235–241.
799 Tobin, H.J., & Kinoshita, M., 2006. Investigations of seismogenesis at the Nankai Trough,
800 Japan. IODP Sci. Prosp. NanTroSEIZE Stage 1.
801 http://dx.doi.org/10.2204/iodp.sp.nantroseize1.2006
802 Tobin, H., Kinoshita, M., Ashi, J., Lallemant, S., Kimura, G., Screaton, E., Moe, K.T., Masago,
803 H., Curewitz, D. & the Expedition 314/315/316 Scientists, 2009a. NanTroSEIZE
804 Stage 1 expeditions: introduction and synthesis of key results. *In* Kinoshita, M.,
805 Tobin, H., Ashi, J., Kimura, G., Lallement, S., Screaton, E.J., Curewitz, D., Masago, H.,
806 Moe, K.T., and the Expedition 314/315/316 Scientists, Proc. IODP 314/315/316:
807 Washington, DC (Integrated Ocean Drilling Program Management International,
808 Inc.). http://dx.doi.org/10.2204/iodp.proc.314315316.101.2009
809 Tobin, H., Kinoshita, M., Moe, K.T., and the Expedition 314 Scientists, 2009b. Expedition
810 314 summary, in *NanTroSEIZE Stage 1:* Investigations of Seismogenesis, Nankai

Trough, Japan, Proc. ICD *314/315/316*, http://dx.doi.org/10.2204/iodp.proc.314315316.111.2009.

Tobin, H.J., Saffer, D.M., 2009. Elevated fluid pressure and extreme mechanical weakness of a plate boundary thrust, Nankai Trough subduction zone. Geology 37, 679–682. http://dx.doi.org/10.1130/G25752A.1.

Tsuji, T., Dvorkin, J., Mavko, G., Nakata, N., Matsuoka, T., Nakanishi, A., Kodaira, S., and Nishizawa, O., 2011a. Vp/Vs ratio and shear-wave splitting in the Nankai Trough seismogenic zone: Insights into effective stress, pore pressure and sediment consolidation, GEOPHYSICS 76, WA71-WA82.

Tsuji, T., et al., 2011b. In situ stress state from walkaround VSP anisotropy in the Kumano basin southeast of the Kii Peninsula, Japan, Geochem. Geophys. Geosyst. 12, Q0AD19, http://dx.doi.org/10.1029/2011GC003583.

Tsuji, T., Kawamura, K., Kanamatsu, T., Kasaya, T., Fujikura, K., Ito, Y., Tsuru, T., Kinoshita, M., 2013. Extension of continental crust by anelastic deformation during the 2011 Tohoku-oki earthquake: The role of extensional faulting in the generation of a great tsunami, Earth and Planetary Science Letters 364, 44-58, http://dx.doi.org/10.1016/j.epsl.2012.12.038.

Tsuji, T., Kamei, R., and Pratt, R.G., 2014. Porepressure distribution of a mega-splay fault system in the Nankai Trough subduction zone: Insight into up-dip extent of the seismogenic zone, Earth and Planetary Science Letters 364, 44-58, http://dx.doi.org/10.1016/j.epsl.2012.12.038.

Wang, K., & Hu, Y., 2006. Accretionary prisms in subduction earthquake cycles: The theory of dynamic Coulomb wedge, J. Geophys. Res. 111, B06410, http://dx.doi.org/10.1029/2005JB004094.

Wu, H.-Y., Kinoshita, M. & Sanada, Y., 2012. Stress state estimation by geophysical logs in NanTroSEIZE Expedition 319-Site C0009, Kumano Basin, southwest Japan, Geophys. Res. Lett. 39, L18303, http://dx.doi.org/10.1029/2012GL053086.

Wu H-Y., Chan, C.-H., Kinoshita, M. & Saito, S., 2013. Stress field observation and modeling from the NanTroSEIZE scientific drillings in the Nankai Trough system, SW Japan, Tectonophysics 600, 99-107. http://dx.doi.org/10.1016/j.tecto.2013.04.009.

Yamada, Y. & Shibanuma, J. 2015. Small-scale stress fluctuations in borehole breakouts and their implication in identifying potential active faults around the seismogenic megasplay fault, Nankai Trough, SW Japan, Earth, Planets and Space, 67, 17, http://dx.doi.org/10.1186/s40623-014-0176-9.

Yamamoto, Yuzuru, Lin, W., Oda, H., Byrne, T., Yamamoto, Yuhji. 2013. Stress states at the

847 subduction input site, Nankai Subduction Zone, using anelastic strain recovery
848 (ASR) data in the basement basalt and overlying sediments, Tectonophysics 600,
849 91-98. http://dx.doi.org/10.1016/j.tecto.2013.01.028.
850
851

852 **Table and Figures' captions**

853

854 Table 1 Specifications of the stress measurement related boreholes in NanTroSEIZE and
855 JFAST drilling sites. For example, C0002 denotes the drilling site; whereas C0002A is
856 the name of the borehole "A" located at Site C0002. Usually, multi boreholes were
857 drilled for different operations within a narrow area (e.g. a few tens meters) in a site in
858 IODP.

859

860 Fig. 1 (1.5-column fitting) Nankai and Japan Trench subduction zones and plates around
861 Japan islands. Red stars and numbers show the epicenters of the earthquakes and
862 its occurrence year; the red frames are the area of rupture zones during the
863 earthquakes. White arrows and numbers show directions and rates of plate motion,
864 respectively (Sella et al., 2002; Apel et al., 2006; Loveless and Meade, 2010; Ozawa
865 et al., 2011).

866

867 Fig. 2 (2-column fitting) Distributions of semi three-dimensional stress state in
868 NanTroSEIZE transect. Codes (e.g. C0009) are the number of drilling sites. Red,
869 black and light blue arrows are the orientations of the maximum, intermediate and
870 minimum principal stresses, respectively. Two pair arrows in the same light blue
871 color in the deeper part of C0009, C0002 and C0012 mean that the intermediate
872 and minimum principal stresses are nearly equal each other, or the intermediate
873 and minimum principal stresses are highly variable.

874

875 Fig. 3 (2-column fitting) Seismic reflection section of NanTroSEIZE transect (modified
876 from Saito et al., 2009). Depths denote the depth below sea level. The gray overlay
877 shows the predicted area of horizontal σ_1 (the maximum principal stress). Around
878 megasplay site C0004 and the frontal thrust site C0006, two patterns of σ_1
879 distribution are considered to be possible. The first one is a gradual change: but the
880 other shows a drastic change around the decollement and the megasplay suggested
881 from the observations at ODP Site 808 and Alaska (Lallemant et al., 1993 and Byrne
882 & Fisher, 1990).

883

884 Fig. 4 (2-column fitting) The maximum horizontal stress (S_{Hmax}) orientations in SW and
885 NE Japan subduction zones. Red bars at the drilling sites show the representative
886 S_{Hmax} orientations in the sites. Two rad rectangles in inset shows locations of figures
887 (a) and (b), respectively. (a) Stress orientations at Site C0009 compiled from Lin et

al. (2010a) and Wu et al., (2012); C0002, C0001, C0004 and C0006 from Chang et al. (2010), C0011 from Expedition 322 Scientists (2010), C0012 from Yamamoto et al. (2013), and at ODP Site 808 from McNeill et al. (2004) and Ienaga et al. (2006). Yellow arrows show the far-field convergence vectors between the Philippine Sea plate and Japan (Heki and Miyazaki, 2001; Miyazaki and Heki, 2001). (b) Location of JFAST Site C0019 and S_{Hmax} orientation in the deep part of the borehole (Lin et al., 2013). Red solid and dashed lines show the mean S_{Hmax} orientation and one standard deviation (SD), respectively, determined in 2012 after the 2011 Tohoku earthquake. Green circles and lines show ODP sites drilled in 1999 and their S_{Hmax} orientations prior to the 2011 earthquake (Lin et al., 2011). The gray arrow shows relative plate motion around Site C0019 (Argus et al., 2011). The white numbers and the contour lines show water depths.

Fig. 5 (2-column fitting) A comparison of seismic reflection profiles of NanTroSEIZE transect and around JFAST drilling site in the same scale (modified from Moore et al., 2009 and Kodaira et al., 2012 respectively) shows the overall similar structures. The five structure horizontal areas, the deep sea terrace, the upper, middle and lower slopes and the trench axis were defined by Kodaira et al. (2012). Site C0006 in the Nankai subduction zone is at the similar location as Site C0019 in the Japan Trench. At exact location of C0019 no wider seismic profile available, thus we used this profile locating just 15 km north of C0019.

Fig. 6 (2-column fitting) A comparison of stress states in the hanging wall of the frontal plate-interfaces in toe of Nankai and Japan Trench subduction zones revealed from Sites C0006 and C0019. (a) Possible stress state at 476 mbsf in borehole C0006B constrained from breakout width and assumed wall rock unconfined compressive strength (UCS) locates in the area of normal faulting stress regime (Wu et al., 2013). (b) Stress state at 468 mbsf in borehole C0006F determined from ASR measurements is of normal faulting stress regime being consistent with that from breakouts in C0006B (Byrne et al., 2009). (c) Possible stress state at 720 mbsf in borehole C0019B constrained from breakout width and measured UCS 3.8 MPa locates in the area of normal faulting stress regime (Lin et al., 2013). (d) Schematic of the current common stress state in the hanging wall of the frontal plate-interfaces in both Sites C0006 and C0019.

Fig. 7 (1.5-column fitting) Schematic of inferred coseismic three-dimensional stress state

924 change from a reverse faulting regime before the Tohoku-oki earthquake (a) to a
925 normal faulting regime after the earthquake (b) in the lower portion of the frontal
926 prism in Japan Trench subduction zone obtained from JFAST (Modified from Lin et
927 al., 2013). NAP denotes North American Plate. Red arrows indicate the maximum
928 principal stress (σ_1); blue arrows: the intermediate principal stress (σ_2); black
929 arrows: the minimum principal stress (σ_3). Because the static vertical stress (σ_v) is
930 under a mechanical equilibrium state with the overburden pressure (the gravity of
931 the formations above the depth), the magnitude of σ_v may not change before and
932 after the earthquake; however was the σ_3 before the earthquake, the σ_1 after the
933 earthquake according to the changes of horizontal stress magnitudes during the
934 earthquake.
935

Table 1 Specifications of the stress measurement related boreholes in NanTroSEIZE and JFAST drilling sites. For example, C0002 denotes the drilling site; whereas C0002A is the name of the borehole "A" located at Site C0002. Usually, multi boreholes were drilled for different operations within a narrow area (e.g. a few tens meters) in a site in IODP.

Holes (stress related operations)	Location		Water depth m	Total depth mbsf	Source of data
	Latitude	Longitude			
C0009A (WL&C*)	33°27.47′N	136°32.15′E	2054	1604	Exp 319 Summary
C0002A (LWD**)	33°18.02′N	136°38.18′E	1936	1402	Exp 314 Summary
C0002B (Coring)	33°17.99′N	136°38.20′E	1938	1057	Exp 315 Summary
C0001D (LWD)	33°14.33′N	136°42.70′E	2198	976	Exp 314 Summary
C0001E (Coring)	33°14.34′N	136°42.69′E	2198	118	Exp 315 Summary
C0001F (Coring)	33°14.34′N	136°42.71′E	2197	249	Exp 315 Summary
C0004B (LWD)	33°13.23′N	136°43.35′E	2637	400	Exp 314 Summary
C0010A (LWD)	33°12.60′N	136°41.12′E	2524	555	Exp 319 Summary
C0006B (LWD)	33°01.64′N	136°47.64′E	3872	886	Exp 314 Summary
C0006E (Coring)	33°01.64′N	136°47.63′E	3876	409	Exp 316 Summary
C0011A (LWD)	32°49.73′N	136°52.89′E	4049	952	Exp 319 Summary
C0012A (Coring)	32°44.89′N	136°55.02′E	3511	576	Exp 322 Summary
C0019B (LWD)	37°56.34′N	143°54.81′E	6890	851	Exp 343 Summary

*WL&C: Wireline logging and coring

**LWD: Logging While Drilling

Figures and their captions

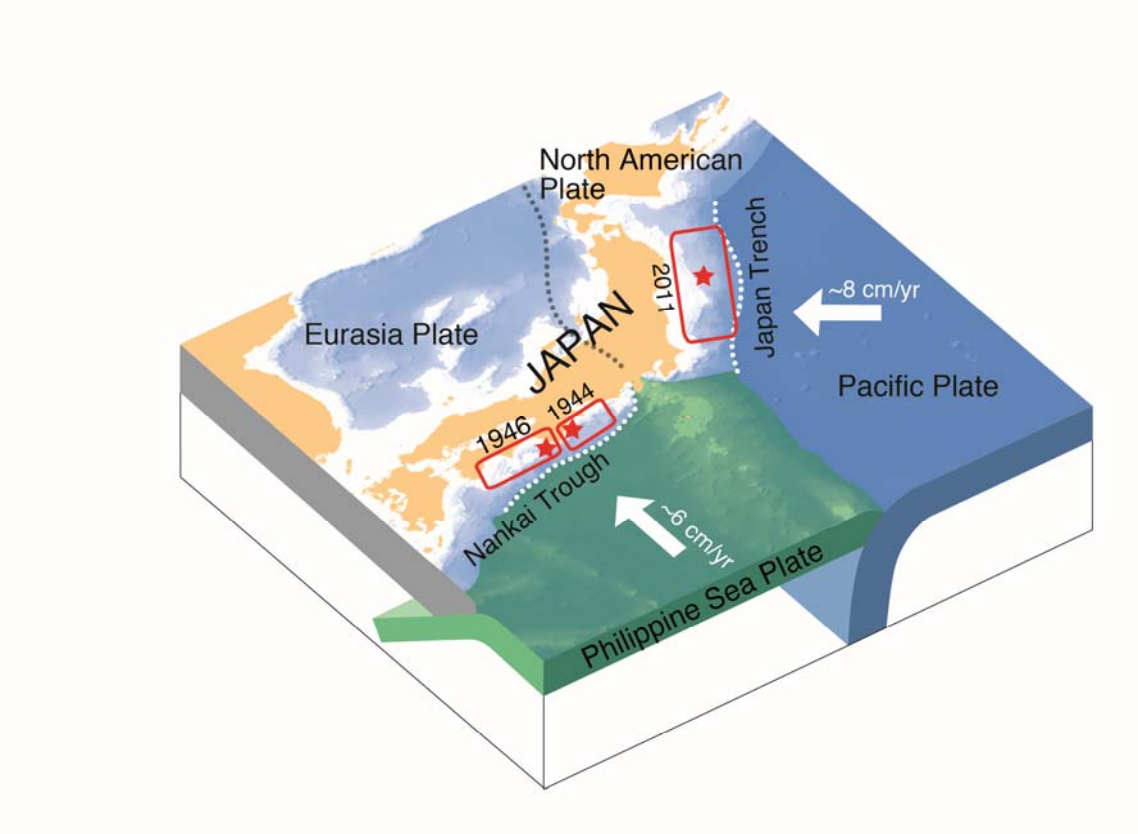

Fig. 1 (1.5-column fitting) Nankai and Japan Trench subduction zones and plates around Japan islands. Red stars and numbers show the epicenters of the earthquakes and its occurrence year; the red frames are the area of rupture zones during the earthquakes. White arrows and numbers show directions and rates of plate motion, respectively (Sella et al., 2002; Apel et al., 2006; Loveless and Meade, 2010; Ozawa et al., 2011).

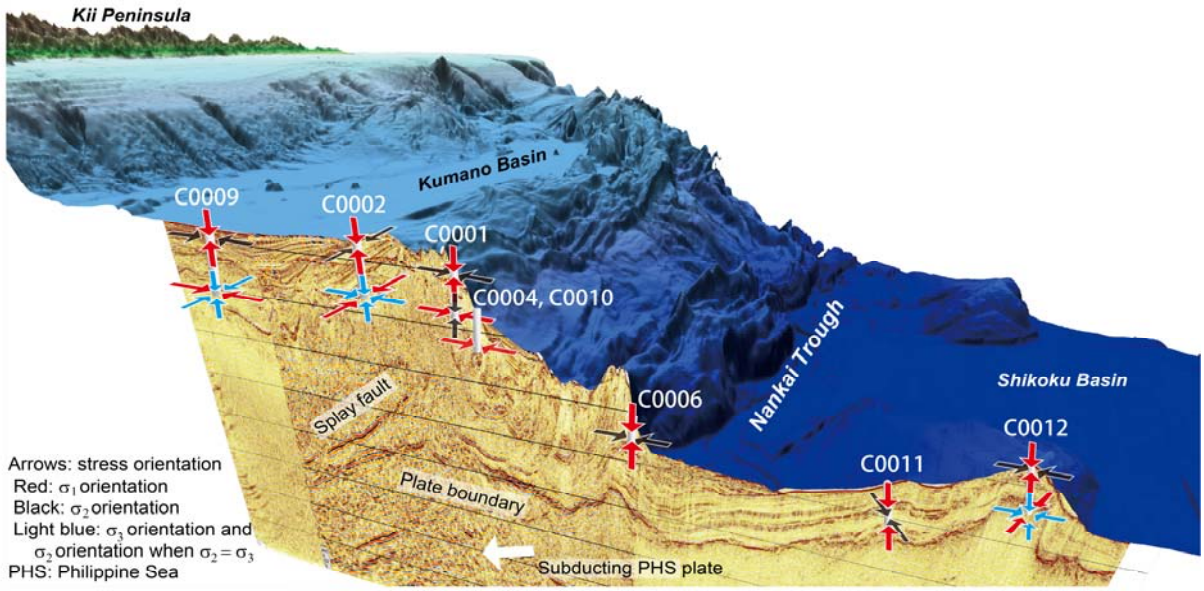

Figure 2 (2-column fitting)

Fig. 2 (2-column fitting) Distributions of semi three-dimensional stress state in NanTroSEIZE transect. Codes (e.g. C0009) are the number of drilling sites. Red, black and light blue arrows are the orientations of the maximum, intermediate and minimum principal stresses, respectively. Two pair arrows in the same light blue color in the deeper part of C0009, C0002 and C0012 mean that the intermediate and minimum principal stresses are nearly equal each other, or the intermediate and minimum principal stresses are highly variable.

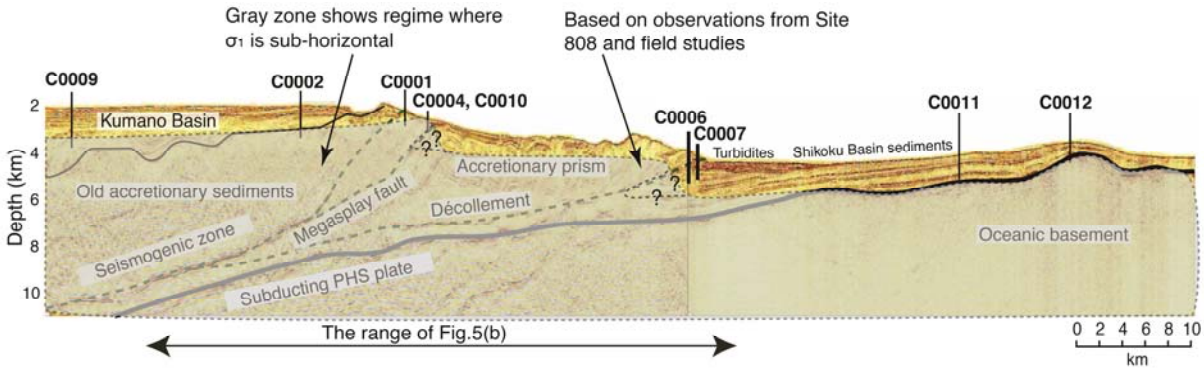

Fig. 3 (2-column fitting) Seismic reflection section of NanTroSEIZE transect (modified from Saito et al., 2009). Depths denote the depth below sea level. The gray overlay shows the predicted area of horizontal σ_1 (the maximum principal stress). Around megasplay site C0004 and the frontal thrust site C0006, two patterns of σ_1 distribution are considered to be possible. The first one is a gradual change: but the other shows a drastic change around the decollement and the megasplay suggested from the observations at ODP Site 808 and Alaska (~~Lallement~~ Lallemant et al., 1993 and Byrne & Fisher, 1990).

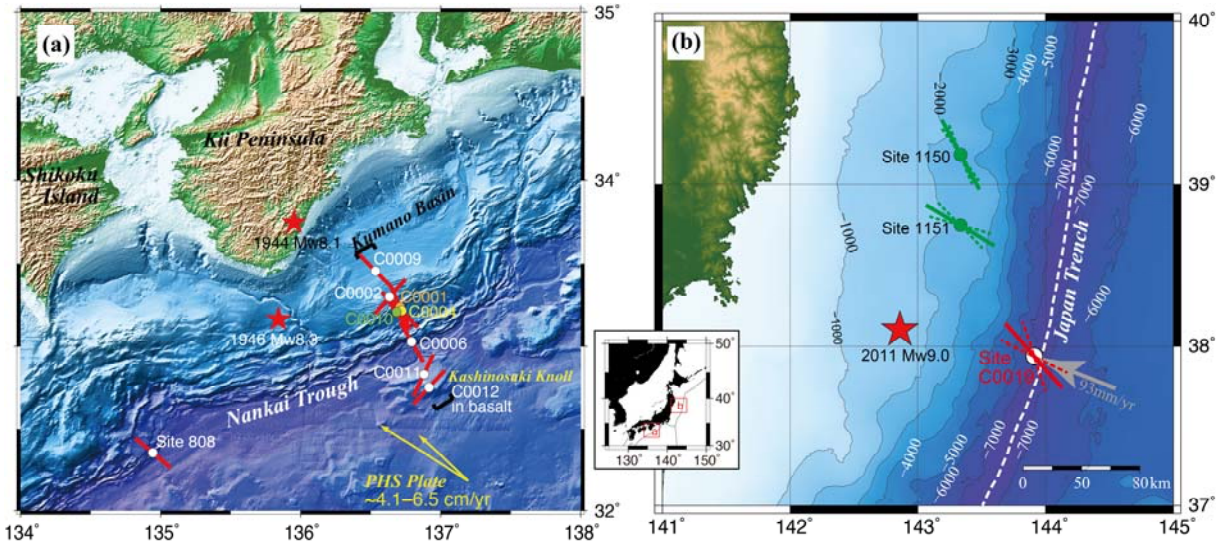

Fig. 4 (2-column fitting) The maximum horizontal stress (S_{Hmax}) orientations in SW and NE Japan subduction zones. Red bars at the drilling sites show the representative S_{Hmax} orientations in the sites. Two rad rectangles in inset shows locations of figures (a) and (b), respectively. (a) Stress orientations at Site C0009 compiled from Lin et al. (2010a) and Wu et al., (2012); C0002, C0001, C0004 and C0006 from Chang et al. (2010), C0011 from Expedition 322 Scientists (2010), C0012 from Yamamoto et al. (2013), and at ODP Site 808 from McNeill et al. (2004) and Ienaga et al. (2006). Yellow arrows show the far-field convergence vectors between the Philippine Sea plate and Japan (Heki and Miyazaki, 2001; Miyazaki and Heki, 2001). (b) Location of JFAST Site C0019 and S_{Hmax} orientation in the deep part of the borehole (Lin et al., 2013). Red solid and dashed lines show the mean S_{Hmax} orientation and one standard deviation (SD), respectively, determined in 2012 after the 2011 Tohoku earthquake. Green circles and lines show ODP sites drilled in 1999 and their S_{Hmax} orientations prior to the 2011 earthquake (Lin et al., 2011). The gray arrow shows relative plate motion around Site C0019 (Argus et al., 2011). The white numbers and the contour lines show water depths.

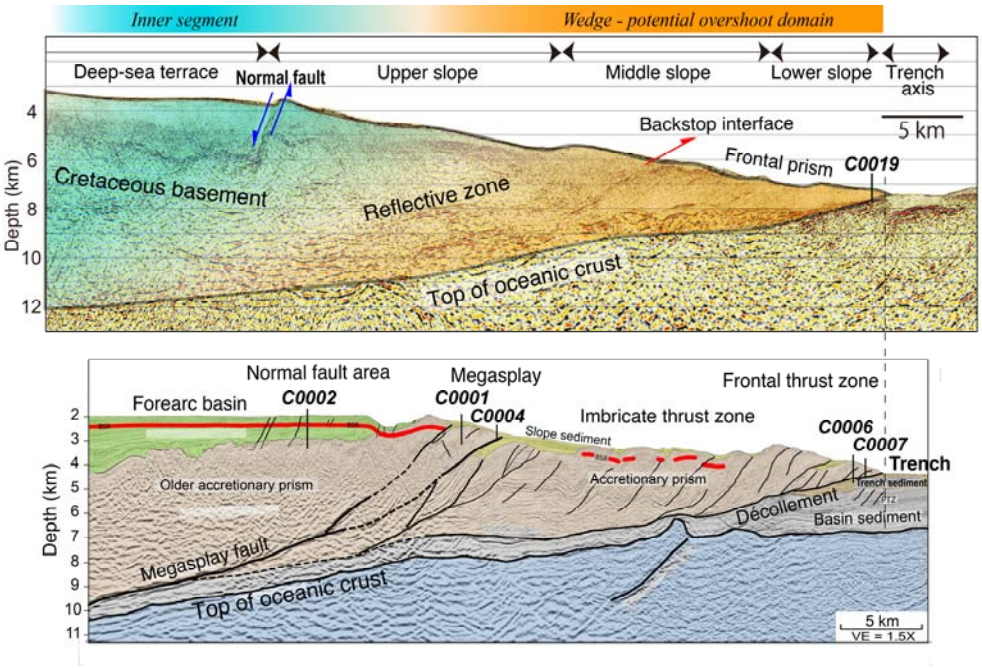

930

931

932 Fig. 5 (2-column fitting) A comparison of seismic reflection profiles of NanTroSEIZE
933 transect and around JFAST drilling site in the same scale (modified from Moore et al.,
934 2009 and Kodaira et al., 2012 respectively) shows the overall similar structures. The
935 five structure horizontal areas, the deep sea terrace, the upper, middle and lower
936 slopes and the trench axis were defined by Kodaira et al. (2012). Site C0006 in the
937 Nankai subduction zone is at the similar location as Site C0019 in the Japan Trench.
938 At exact location of C0019 no wider seismic profile available, thus we used this
939 profile locating just 15 km north of C0019.

940

941

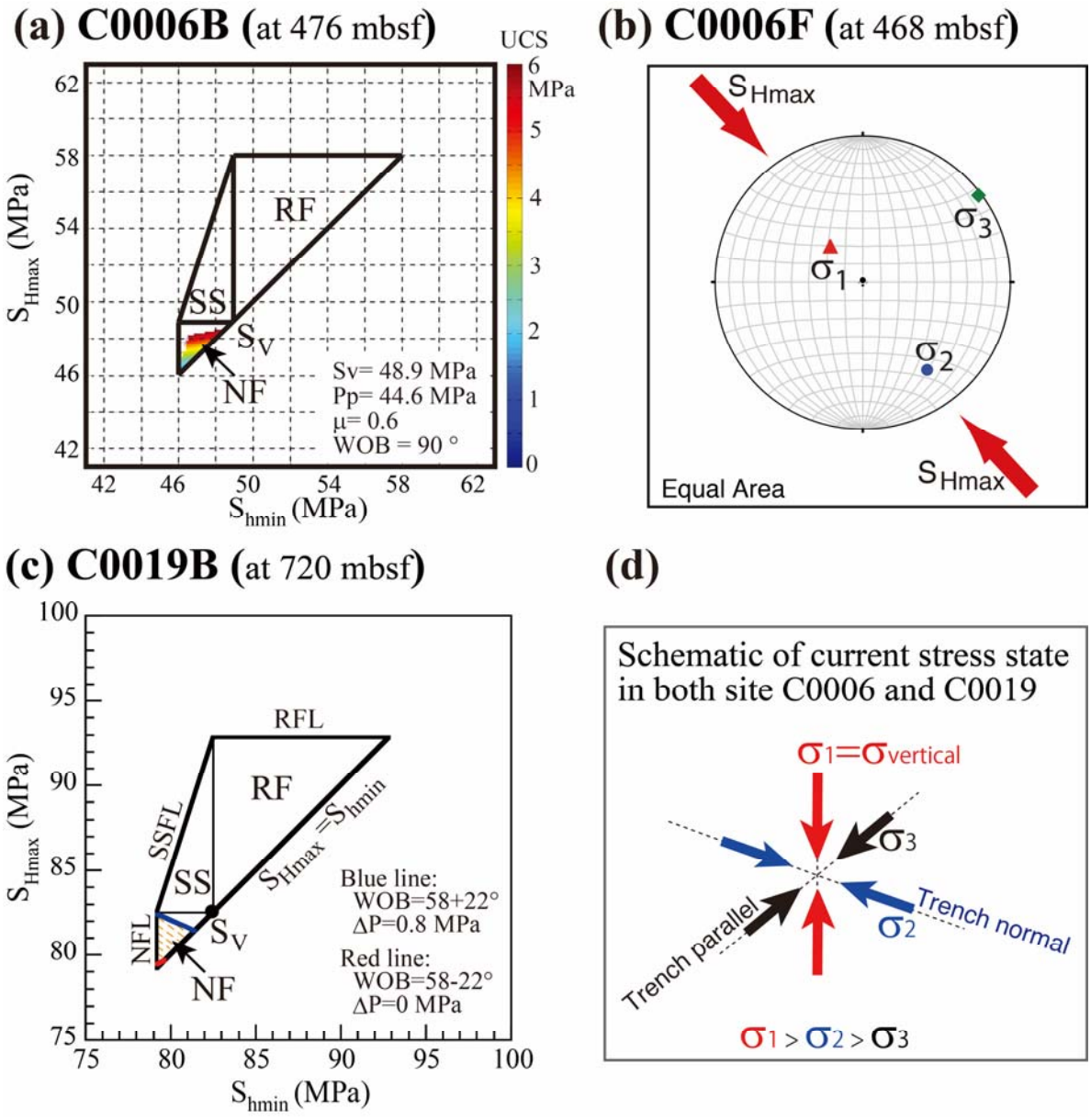

Fig. 6 (2-column fitting) A comparison of stress states in the hanging wall of the frontal plate-interfaces in toe of Nankai and Japan Trench subduction zones revealed from Sites C0006 and C0019. (a) Possible stress state at 476 mbsf in borehole C0006B constrained from breakout width and assumed wall rock unconfined compressive strength (UCS) locates in the area of normal faulting stress regime (Wu et al., 2013). (b) Stress state at 468 mbsf in borehole C0006F determined from ASR measurements is of normal faulting stress regime being consistent with that from breakouts in C0006B (Byrne et al., 2009). (c) Possible stress state at 720 mbsf in borehole C0019B constrained from breakout width and measured UCS 3.8 MPa locates in the area of normal faulting stress regime (Lin et al., 2013). (d) Schematic of the current common stress state in the hanging wall of the frontal plate-interfaces in both Sites C0006 and C0019.

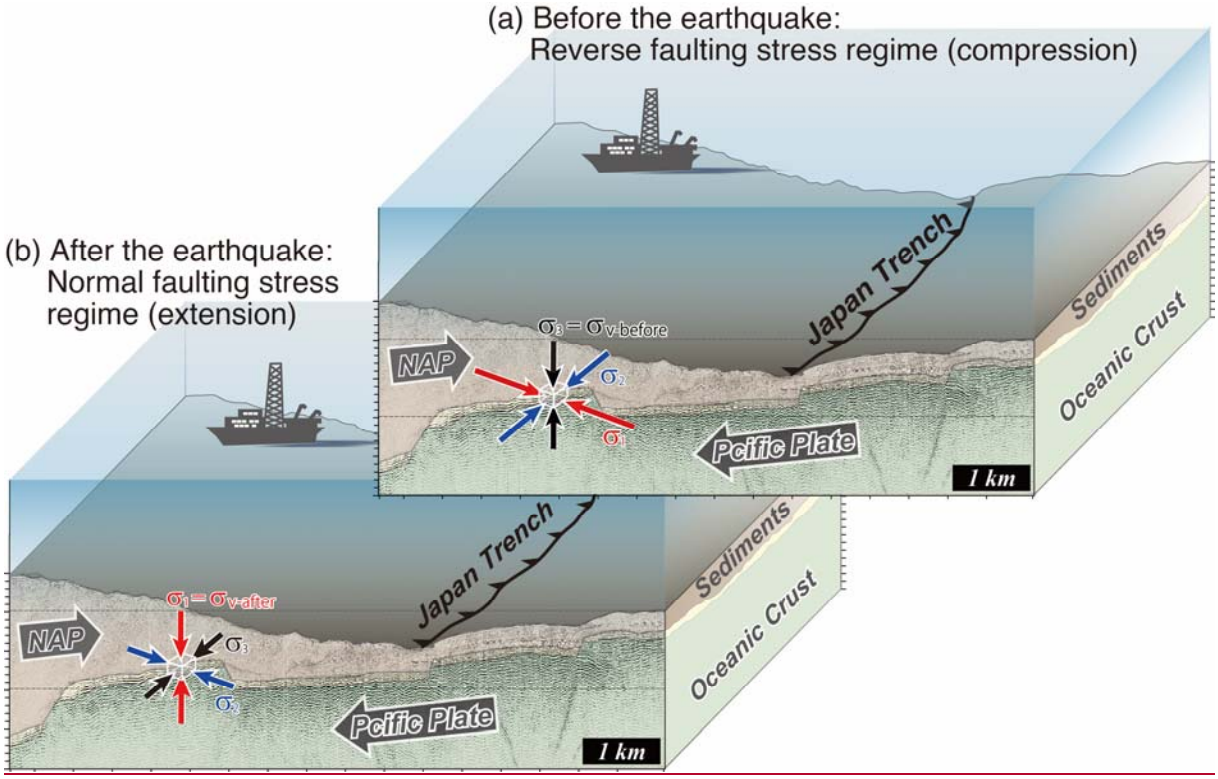

Fig. 7 (1.5-column fitting) Schematic of inferred coseismic three-dimensional stress state change from a reverse faulting regime before the Tohoku-oki earthquake (a) to a normal faulting regime after the earthquake (b) in the lower portion of the frontal prism in Japan Trench subduction zone obtained from JFAST (Modified from Lin et al., 2013). NAP denotes North American Plate. Red arrows indicate the maximum principal stress (σ_1); blue arrows: the intermediate principal stress (σ_2); black arrows: the minimum principal stress (σ_3). Because the static vertical stress (σ_v) is under a mechanical equilibrium state with the overburden pressure (the gravity of the formations above the depth), the magnitude of σ_v may not change before and after the earthquake; however was the σ_3 before the earthquake, the σ_1 after the earthquake according to the changes of horizontal stress magnitudes during the earthquake.